Agricultural and Forest Meteorology 362 (2025) 110373

Contents lists available at ScienceDirect

Agricultural and Forest Meteorology

journal homepage: www.elsevier.com/locate/agrformet

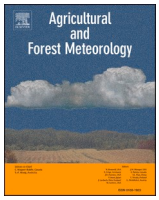

# The biophysical effects of phenological shifts impact land surface temperature for corn expansion in Northeastern China

Yuyang Ma [a], Jie Li [a,*], Jianxi Huang [b,c], Anne Gobin [d,e], Xuecao Li [b,c], Wenqi Liu [h], Haixiang Guan [b], Nadezhda N. Voropay [f,g], Chuli Hu [a]

[a] College of Geography and Information Engineering, China University of Geosciences, Wuhan 430074, PR China
[b] College of Land Science and Technology, China Agricultural University, Beijing 100083, PR China
[c] Key Laboratory of Remote Sensing for Agri-Hazards, Ministry of Agriculture and Rural Affairs, Beijing 100083, PR China
[d] Flemish Institute for Technological Research (VITO NV), Boeretang 200, B-2400 Mol, Belgium
[e] Department of Earth and Environmental Sciences, Faculty of Bioscience Engineering, University of Leuven, Celestijnenlaan 200E, 3001 Leuven, Belgium
[f] Institute of Monitoring of Climatic and Ecological Systems, Siberian Branch, Russian Academy of Sciences, 634055, Tomsk, Russia
[g] Sochava Institute of Geography, Siberian Branch, Russian Academy of Sciences, 664033, Irkutsk, Russia
[h] Department of Geography, Oklahoma State University, Stillwater, OK 74075, USA

ARTICLE INFO

*Keywords:*
Phenology
Corn expansion
Biophysical effects
Land surface temperature
Surface energy balance

ABSTRACT

In the last two decades, rapid corn expansion has significantly impacted local and regional climates in Northeastern China. However, its climatic effects and underlying biophysical mechanisms have rarely been investigated, particularly in accurately describing the changes in surface physiological structure throughout different phenological stages. This study utilized remote sensing observations and the pair-wise comparison approach to examine land surface temperature (LST) change associated with corn expansion at various phenological stages and whole growth seasons, respectively. We then employed the temperature response model to decompose and quantify the LST changes into radiative processes (albedo) and non-radiative processes (i.e., evapotranspiration and turbulent heat exchange). This study indicated that, except for soybean, the mean LST changes (ΔMean_LST) induced by corn expansion initially decreased and subsequently increased with the phenology shifts. Specifically, the potential warming effect was pronounced during three-leaves (EMV3) to seven-leaves stage (V7) and V7 to jointing date (JD), with the largest warming in Mean_LST occurring when corns were converted into trees (1.24 ±0.43 K) (mean ± 95 % confidence level) (0.93±0.29 K), followed by grass (0.47±0.37 K) (0.43±0.31 K), rice (0.46±0.23 K) (0.31±0.22 K), wetlands (0.16±0.21 K) (0.15±0.34), respectively. EMV3 to JD dominated the ΔMean_LST for the whole growth season, potentially warming the Mean_LST when trees, grass, rice, and wetlands converted to corn, while cooling the Mean_LST when soybeans converted to corn. Furthermore, The effect of phenological stages on LST varies with latitude. For example, during V7 to JD and Milky date (MID) to Maturity date (MD), the non-radiative warming effect of wetland conversion surpassed that of rice conversion as latitude increased (44°N-47°N). This indicates that the wetland conversion causes intensified warming at high latitudes in these stages. Additionally, non-radiative processes, characterized by varying signs and magnitudes, dominated the LST response to corn expansion. Overall, this study comprehensively investigated the ΔLST of corn expansion at various phenological stages and latitudes through the biophysical mechanism, which could be beneficial in developing adaptive and mitigative agricultural management strategies for climate warming in Northeast China.

## 1. Introduction

Crop phenology is an indicator of agricultural ecosystem responses to climate change (Liu et al., 2017; 2022; Piao et al., 2019; Zhao et al., 2023). It affects the exchange of carbon, water, and energy between vegetation and the atmosphere through biogeochemical and biogeophysical processes. Biogeochemical processes associated with changes in $CO_2$ and $CH_4$ emissions are usually performed globally and

* Corresponidng author.
*E-mail address:* lijie_gis@cug.edu.cn (J. Li).

https://doi.org/10.1016/j.agrformet.2024.110373
Received 7 October 2024; Received in revised form 23 November 2024; Accepted 18 December 2024
Available online 27 December 2024

require multi-decadal (Graven et al., 2013; Liu et al., 2019a). Biogeophysical processes can directly influence the atmosphere via land surface energy balance at local and regional scales (Chen et al., 2020; Lee et al., 2011; Zeng et al., 2017). For instance, crop emergence, leaf expansion, flowering, and maturity alter crop height, canopy structure, and leaf color, thereby affecting surface albedo and roughness, dividing between latent and sensible heat flux, which subsequently regulates local climate (Zeng et al., 2023; Zhao et al., 2023; Zhou et al., 2021). Consequently, these periodic variations of crop phenology may influence future climate changes in complicated agroecosystems.

Numerous studies have investigated the biophysical mechanisms of the crops and natural vegetation greening that affect land surface temperature (LST) (Chen et al., 2020; Yu et al., 2022; Zhao et al., 2023). For example, crop greening mitigates climate warming in mid-high latitudes, with aerodynamic and surface resistance being the primary factors contributing to the decreases in

LST (Yu et al., 2022). Chen et al. (2020) revealed that earth greening decreases LST via increasing LAI, which reduces aerodynamic resistance and facilitates enhanced turbulent heat transfer between ground and atmosphere, particularly latent heat flux. These studies highlighted the LST change and feedback mechanism of greening on climate over a long time series. Numerous studies focused on investigating the potential biophysical effects of natural vegetation converting to crops on climate at month, season, and year time scales, including paddy field expansion, irrigated cropland, and wetland degradation (Bright et al., 2017; Liu et al., 2018; 2022). For instance, studies have shown that rice expansion and wetland restoration could decrease LST, which is dominated by nonradiative processes (i.e., evapotranspiration and sensible heat) (Liu et al., 2019b). They regarded rice fields as artificial wetlands comparable to low vegetation cover flooded areas, which can mitigate the warming impacts caused by wetland degradation (Liu et al., 2019a; 2022). However, the greening of the wetlands occurs before the transplanting of rice, and whether its biophysical impacts on LST are completely constant remains uncertain, which is related to phenological shifts and has not been previously investigated. It is critical for agroecosystems and regional climate. Moreover, grassland has been used as a proxy for crops in the majority of integrated vegetation climate modeling experiments (Levis, 2010; Zhao et al., 2023). Nevertheless, there are significant differences in their structural, physiological, and phenological characteristics. For instance, grassland emerges earlier than crops at mid-high latitudes. The LAI peak value of crops (such as corn, soybeans, and rice) exceeded that of grassland over the whole growing season (Zhao et al., 2023). Nevertheless, these studies overlooked phenological shifts, such as changes in crop height and canopy density, resulting in LST changes by affecting the solar radiation absorption and energy diffused through turbulence, which modifies biophysical feedback and introduces significant uncertainties in crop responses to climate. Thus, it is imperative to investigate the LST variations and biophysical mechanism differences between crops and vegetation at various phenological stages.

Northeast China (Heilongjiang, Jilin, and Liaoning) is a typical agroecosystem that has experienced considerable warming over the past few decades (Zhou et al., 2021). Annual sunshine hours have decreased by 40.6 h per decade, and the daily minimum temperature has increased more significantly than the daily maximum temperature, hence narrowing the diurnal temperature range (Li et al., 2016). This could modify plant photosynthesis and respiration, leading to negative impacts on the accumulation of organic compounds (Yu et al., 2022). Consequently, it is essential to investigate the reasons for warming. Although numerous studies have focused on rice expansion decreasing LST through non-biological physical processes in Northeast China (Liu et al., 2019a; 2022; Zhang et al., 2022), this cannot explain the persistent warming. It is worth noting that the expansion of corn is 2.19 times greater than that of rice, increasing from 5.42 $\times$ $10^3$ $km^2$ to 127.19 $\times$ $10^3$ $km^2$ between 2000 and 2017 (http://www.stats.gov.cn/sj/ndsj/, accessed on 2 October 2024), and continues to rise at an average annual increase rate of 4042 $km^2$, primarily at the expense of grasslands, trees, and wetlands. However, to our knowledge, few studies have investigated the biophysical mechanism influencing LST, particularly across different phenological stages, which is crucial for understanding regional diurnal LST and its driving mechanisms.

The biophysical effects of vegetation type conversion on climate are primarily assessed by climate model simulations, site measurements, and remote sensing observations (Chai et al., 2024; Duveiller et al., 2018; Lee et al., 2011; Liu et al., 2022; Zeng et al., 2017; Zhang et al., 2023b). Climate models can simulate the large- and regional-scale biophysical effects of vegetation-type conversion through controlled experiments that include and exclude such conversion, but there are uncertainties in physical processes, parameterization, and input data. Site observations provide precise measurements and comparisons of vegetation type conversions, but they are difficult to upscale in larger regions due to limited data availability, particularly in agroecosystems (Lee et al., 2011; Liu et al., 2017). Pair-wise comparison utilizing remote sensing observation is an effective method for identifying the climate effect, assuming that the target and the nearby vegetation type share the same background climate. This quantifies the relative contributions of radiative forcing (albedo) and non-radiative processes (evaporation and turbulent heat exchange) through the energy budget balance (Bright et al., 2017; Liu et al., 2019a).

To this end, this study aims to investigate the impact of corn expansion at various phenological stages on LST and to clarify its biophysical mechanisms. Satellite measurements were utilized to demonstrate the impact of corn expansion on LST in various phenological stages with latitude changes. A pair-wise comparison was utilized to elucidate the LST changes in various phenological stages during diverse vegetation conversions to corn (each phenological stage of corn is regarded as a sub-vegetation type). Finally, the temperature response model was employed to explain the divergent biophysical mechanisms of corn expansion in various phenological stages. This study highlights the role of phenology shifts and latitude changes in regulating the LST on corn expansion. It contributes to developing adaptive and mitigative agricultural management strategies in Northeast China for climate warming situations.

## 2. Materials and methods

### 2.1. Study area

This study was performed in Northeast China and extended from 38.62°N to 45.93°N latitude and 118.83°E to 135.10°E longitude. Situated in a temperate continental climate with annual precipitation of 500–750 mm and an average annual temperature ranging from 2 °C to 13 °C (Guan et al., 2022). The land cover type includes cropland, grasslands, wetlands, and trees (Fig. 1a). Over the past two decades, an enormous amount of grassland (Fig. 1d) and trees (Table. S1) have been converted to cropland (Ning et al., 2018), making cropland as the dominant land cover type. Corn has rapidly expanded with an average annual growth rate of 4042 $km^2$ and is the widest distribution (12.72 $\times$ $10^4$ $km^2$, in 2017) (Fig. 1b). It has a bigger planted area than rice (5.26 $\times$ $10^4$ $km^2$) and soybean (4.40 $\times$ $10^4$ $km^2$) (https://www.stats.gov.cn/sj/ndsj/2018/indexch.htm, accessed on 2 October 2024).

Furthermore, the characteristics of corn and various vegetation cover types exhibit significant variation throughout stages. The sowing intervals for corn and soybean are approximately 10 days. Corn is planted from early to mid-May, while soybeans are sown in late May, making a longer bare soil window for soybean fields (Liu et al., 2022). Rice has to be initially cultivated in a greenhouse, and the fields were flooded in mid-May and transplanted in late May. Conversely, natural vegetation, such as trees, grasslands, and wetlands green up in early April. Thus, surface biophysical characteristics experienced significant changes due to extensive corn expansion resulting from phenological shifts and management practices.

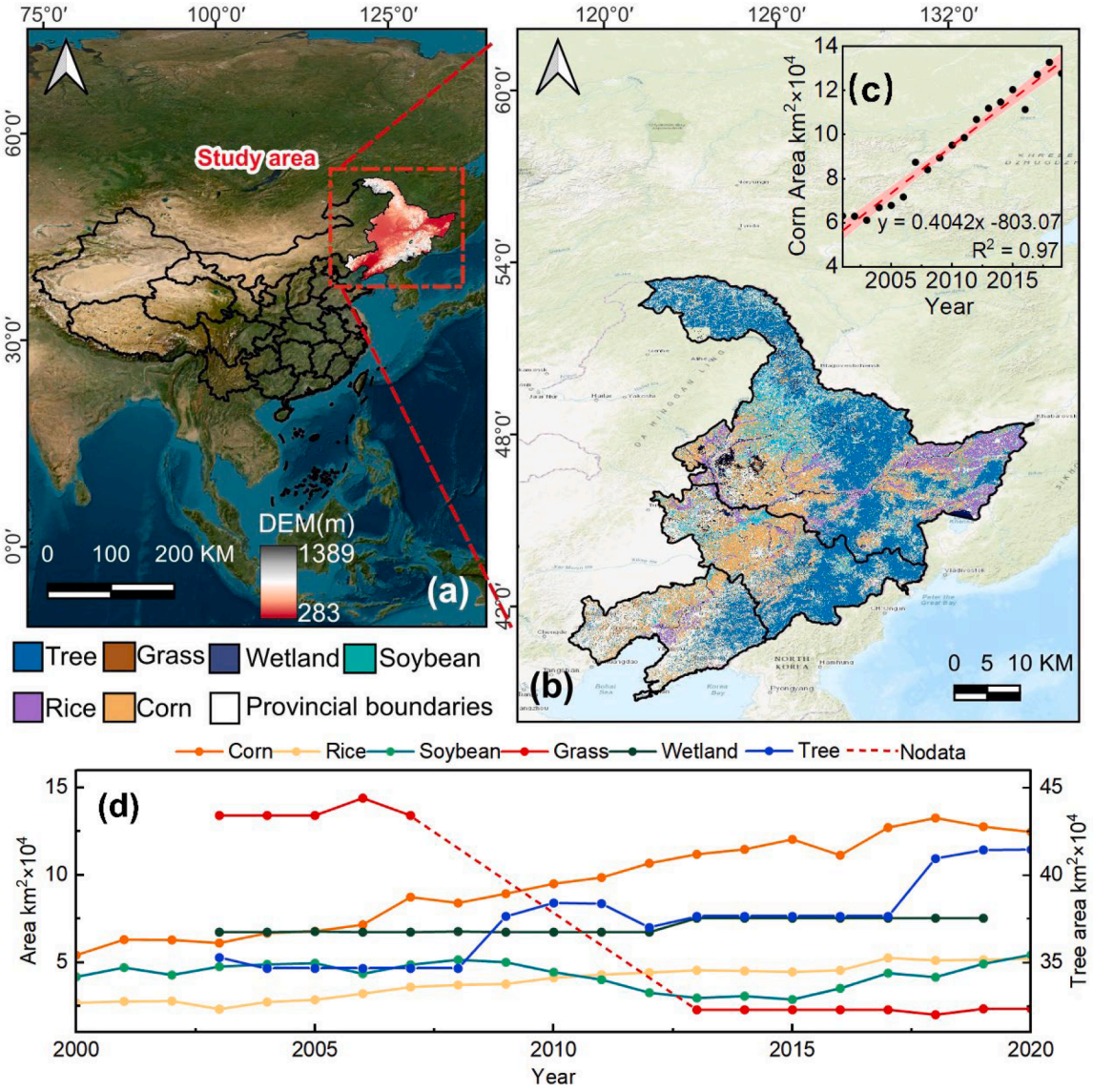


**Fig. 1.** Landcover types in Northeast China, 2017. (a) Location of the study region in northeast China, (b) spatial distribution of major landcover types in northeast China, (c) the annual increase rate of corn planting area from 2000 to 2017, (d) the area of various land cover types in the study area from 2000 to 2020. The left y-coordinate represents the area of corn, rice, soybean, grass, and wetlands. The right y-axis represents the area occupied by trees. The left y-coordinate ranges from 1 to 16, while the right y-axis spans from 31 to 46. The scale for trees and other vegetation is consistent on both axes, facilitating comparisons.

Additionally, as illustrated in Fig. 1d, the area of grass decreased ($-11.06$ km$^2$ $\times$ $10^4$) significantly from 2003 to 2018, while corn (6.35 km$^2$ $\times$ $10^4$) and tree (6.18 km$^2$ $\times$ $10^4$) areas notable increases, rice (2.90 km$^2$ $\times$ $10^4$) and wetland (0.80 km$^2$ $\times$ $10^4$) areas moderate increases. This indicated that grass could be a primary factor in the expansion of corn area. Furthermore, the decreased soybeans area could be converted to a corn area as a result of the soy-corn rotation system implemented from 2010 to 2015 in the study area. Moreover, we investigated existing studies revealed that the conversion rate from wetland to dryland was the highest, followed by grassland, trees, and bareland (Huang et al., 2010; Man et al., 2016). Therefore, this study compared the LST of corn with that of wetlands, grasslands, trees, rice, and soybeans.

### 2.2. Satellite data processing

To investigate the change in biophysical mechanism and LST associated with corn expansion (Conversion from soybean, rice, grass, tree, and wetland). This study extracted all available remote sensing data from April to October from 2017 to 2019. First, this study acquired the Land Surface Temperature (LST) and Emissivity products from the MODIS Land Surface Temperature/Emissivity Daily Version 6.1 product (MOD11A1.061), which has a temporal resolution of one-day and a spatial resolution of 1 km, and employed linear interpolation to fill in missing pixel values (Li et al., 2018). The MODIS LST datasets include mid-daytime (1:30pm, Day_LST) and mid-nighttime (1:30am, Night_LST) observations. This study calculated the average values of Day_LST and Night_LST observations to obtain the mean LST (Mean_LST) in the study area. The albedo data is the MCD43A3 version 6.1 albedo model dataset (MCD43A3.061), produced daily using 16 days of Terra and Aqua MODIS data at 500 m resolution. The albedo data include black-sky albedo (directional hemispherical reflectance) and white-sky albedo (bi-hemispherical reflectance) for shortwave broadband (Román et al., 2010; Schaaf et al., 2002). This study calculated the mean to assess real conditions, avoiding the influence of diffuse radiation fractional information (Liu et al., 2022).

Furthermore, this study acquired daily downward shortwave radiation, downward longwave radiation, and 2 m air temperature from the enhanced global dataset for the land component of the fifth generation

of European reanalysis (ERA5_land), which has a spatial resolution with 0.1° × 0.1° (Yang et al., 2006), and has been widely validated and utilized in Northeast China and other regions (Fang et al., 2021; Gong et al., 2022; McNicholl et al., 2021; Xin et al., 2021). Although there are other relevant data available (Chen Yingying, 2015; He et al., 2020; Yang et al., 2010), they have not been adopted in this study owing to the considerable block effects in station data interpolation, which would increase uncertainty. Moreover, ERA5_land provided a consistent view of the water and energy cycles at the surface level for several decades. The ERA5_land with a one-day temporal resolution, is crucial for examining surface energy balance in various phenological stages, as most phenological stages endure only one to two weeks. All remote sensing data are utilized to estimate surface energy redistribution factors and to divide temperature response processes into radiative or non-radiative processes.

To assess the variation in LST and biophysical mechanisms across different phenological stages in corn expansion. This study obtained 30-m resolution phenological data with an accuracy of 96 %, and the average RMSE for each phenological stage was 8.46 days from 2017 to 2019 according to our improved studies (Ma et al., 2023). The phenology stage included three-leave date (EMV3), seven-leave date (V7), jointing date (JD), tassel date (TD), milky date (MID), and maturity date (MD). Moreover, this study gathered data on crop types and land use types. The 10-m crop map included corn, soybean, and rice in northeast China, with an overall accuracy of 91 % (You et al., 2021). Grass and tree layers were acquired from the ESRI 10 m annual Land Use Land Cover (ESRI_LULC) and annual China Land Cover Dataset (CLCD). ESRI_LULC was derived from Sentinel-2 images at 10 m resolution, with each maps exhibiting an assessed average accuracy over 75 % (Karra et al., 2021). CLCD was produced from the Landsat images with 30 m resolution, achieving an overall accuracy reached 79.31 % (Yang and Huang, 2021). This study extracted the intersection of two datasets to achieve improved precision in grass and tree layers. Moreover, this study also extracted the intersection of the East Asian 10 m resolution Wetland spatial distribution Dataset (EAWD) and CLCD to produce a more accurate wetland layer. The EAWD was extracted from multi-source reference data and Sentinel-1/2 time series remote sensing images, with an accuracy exceeding 88 % (Mao et al., 2020). The crop and land use layers were aggregated to generate 1-km plant area proportion maps (i.e., corn, soybean, rice, grass, tree, and wetland) to align with the spatial resolution of other satellite remote sensing data (Liu et al., 2019a; 2022). Subsequently, single vegetation-type pixels that exceed 80 % within a 1-km grid were filtered. These pixels represent pure pixels of a specific vegetation type (Liu et al., 2022).

Additionally, to compare the differences in the vegetation surface. This study extracted the leaf area index (LAI) data from The MCD15A3H Version 6.1 Moderate Resolution Imaging Spectroradiometer Level 4 (MCD15A3H.061) (Yang et al., 2006), which was produced by the optimal pixel from all the acquisitions of both MODIS sensors located on Terra and Aqua satellites within 4-days. LAI predominantly governs the biophysical feedback by influencing the absorption of solar radiation through alterations in albedo and the magnitude of evapotranspiration via canopy resistance (Kala et al., 2014).

Table 1

### 2.3. Temperature response model

LST is greatly impacted by energy redistribution through convection and evaporation (Bright et al., 2017; Lee et al., 2011; Liu et al., 2019a). Energy redistribution factor ($f$) expression was proposed by (Lee et al., 2011), integrating aerodynamic and physiological governing surface energy budgets. A higher value of the $f$ corresponds to higher efficiency in nonradiative processes. The formula could be calculated as:

$$f = \frac{\lambda_0}{\mathrm{Ts} - \mathrm{Ta}}\left(R_n^* - G\right) - 1 \quad (1)$$

where $\lambda_0$ is mean Planck response of each phenological stage to the external radiative forcing at the surface calculated as $1/4\varepsilon_s\sigma T_s^3$. $\varepsilon_s$ is mean the surface emissivity in each phenological stage, which is extracted from MOD11A1.061. $T_s$ is each phenological stage mean LST (K). $T_a$ is each phenological stage mean air temperature at 2 m (K). $G$ is each phenological stage mean soil heat flux, which is estimated as 0.14 × ($T_{a,n}$- $T_{a,n-1}$), where $n$ is the phenological stages (V3, V7, JD, TD, MID, MD). $R_n^*$ is mean apparent net radiation of each phenological stage, which can be calculated as:

$$R_n^* = (1-\alpha) \times S + L_{\downarrow} + \sigma T_a^4 \quad (2)$$

where $\alpha$ is mean surface albedo for each phenological stage; $S$ is mean downward shortwave radiation flux for each phenological stage, $(1-\alpha) \times S$ means net shortwave radiation flux, $L_{\downarrow}$ is mean downward longwave radiation flux of each phenological stage. $\sigma$ is the Stefan-Boltzmann constant.

The temperature response model aims to quantify the biophysical effects arising from spatial patterns of vegetation cover sharing the a uniform background climate. Utilizing a linearization of the surface

**Table 1**
Summary of the remote sensing data and products used in this study.

| Dataset | Indicator | Spatial resolution | Temporal resolution | Source | Reference |
|---|---|---|---|---|---|
| MCD43A3.061 | Albedo | 500m | Daily | https://developers.google.com/earth-engine/datasets/catalog/MODIS_061_MCD43A3 | (Shuai et al., 2008) |
| MOD11A1.061 | Emissivity | 1km | Daily | https://developers.google.com/earth-engine/datasets/catalog/MODIS_061_MOD11A1#bands | (Wan, 2014) |
| LST | LST | 1km | Daily | https://gee-community-catalog.org/projects/daily_lst/ | (Li et al., 2018) |
| ERA5_land | Downward shortwave radiation, Downward longwave radiation, 2 m air temperature | 0.1° | Daily | https://developers.google.com/earth/engine/datasets/catalog/ECMWF_ERA5_LAND_DAILY_AGGR | (Muñoz-Sabater et al., 2021) |
| Crop type map | Corn, Soybean, Rice | 10m | — | https://doi.org/10.1038/s41597–021–00827–9 | (You et al., 2021) |
| ESRI_LULC | Grass, Tree | 10m | Yearly | https://gee-community-catalog.org/projects/S2TSLULC/ | (Karra et al., 2021) |
| CLCD | Grass, Tree, Wetland | 30m | Yearly | https://doi.org/10.5281/zenodo.4417810 | (Yang and Huang, 2021) |
| EAWD | Wetland | 10m | — | National Earth System Science Data Center (https://www.geodata.cn) | (Mao et al., 2020; Wang et al., 2023a; 2023b) |
| Corn phenology map | V3, V7, JD, TD, MID, MD | 10m | — | — | (Ma et al., 2023) |
| MCD15A3H.061 | LAI | 500m | 4-Day | https://developers.google.com/earth-engine/datasets/catalog/MODIS_061_MCD15A3H | (Yang et al., 2006) |

longwave radiation term of the surface energy balance equation, Bright et al. (2017) formulated an analytical expression to estimate the direct surface temperature response to vegetation cover conversion, isolating the contribution of each biophysical factor to the predicted LST change ($\Delta T_s$) as follow:

$$\Delta T_s = \frac{\lambda_0}{(1+f)}\Delta R_n^* + \frac{-\lambda_0}{(1+f)}\Delta G + \frac{-\lambda_0}{(1+f)(1+f+\Delta f)}\left(R_n^* - G\right)\Delta f \quad (3)$$

where $\Delta T_s$ is the approximated response to vegetation cover change from type $i$ to type $j$. This study assumes that $R_n^*$, $f$, and $G$ are parameters affected by the vegetation types (corn, rice, soybean, grass, tree, and wetland) in various phenological stages and are independent of $T_s$ (Bright et al., 2017; Liu et al., 2022). Thus, the first, second, and third right-hand terms in Eq. (3) are the response to the surface radiative forcing from the albedo change ($\Delta T_s\_Alb$), the change in heat conducted by the surface medium ($\Delta T_s\_G$), and the change in turbulent energy redistribution ($\Delta T_s\_f$) in each phenological stage, respectively.

### 2.4. Pair-wise comparison

This study aims to quantitatively investigate the impacts of corn expansion on LST at the various phenological stages. Each phenological stage of corn is regarded as a sub-vegetation type in pair-wise comparison to clarify LST changes among various phenological stages of corn and land surfaces. The pair-wise comparison that is, the space-for-time approach, which compared LST changes between corn and various vegetation at the same time to reveal the potential impact of corn expansion on surface temperature (Abera et al., 2020; Bouvet et al., 2018). Notably, the pair-wise comparison method is performed under two assumptions. First, the adjacent vegetation types share the same background state characterized by the incoming solar radiation, the incoming longwave radiation, and air temperature at the blending height. Second, the perturbation signals, such as corn expansions, significantly exceed the background changes (Lee et al., 2011). The elevation disparity between the two vegetation types should be under 100 m to minimize the effect of spatial heterogeneity caused by the atmospheric background (Liu et al., 2022). Furthermore, the sampling region should be sufficient pure pixels for both vegetation types, and the vegetation pixel paired with corn should not be <10 % (Wang et al., 2021). This study extracted samples from three years to compare corn with rice (560), soybean (166), tree (34), grass (121), or wetland (366), respectively. Moreover, this study mainly compared paired pixels utilizing 5 × 5 km sampling areas appropriate for regional studies (Liu et al., 2022; Zhang et al., 2023b). Moreover, to address the phenological stage disparity between crops, this study assumes that the phenology of the two crop types does not change on adjacent dates. Specifically, this study differentiated the phenological stage to each day and calculated the LST changes (ΔLST) of different crops on two consecutive days. Fig. S2 displayed the ΔLST_Alb, and ΔLST_f, ΔMean_LST, diurnal LST range (DTR_LST), ΔDay_LST, and ΔNight_LST at daily scale in the whole growing season. Then the mean of the daily Day_LST, Night_LST, Mean_LST, and DTR_LST of the paired pixels between the two phenological stages was calculated to investigate the growing season and various phenological stages. Mean_LST was calculated using the arithmetic mean of Day_LST (maximum) and Night_LST (minimum). DTR_LST was derived from the difference between Day_LST and Night_LST. This study also compared the albedo and $f$ of paired pixels, together with their magnitude and direction, to illustrate the driving mechanism of the LST change.

## 3. Results

### 3.1. LAI differences between corn and various land surfaces in the growing season

The LAI between corn and other vegetations (rice, soybean, tree, grass, wetland) exhibited significant differences in the growing season (Fig. 2). Corn has a higher LAI value than rice and soybeans, except for the stage from TD to MID (210 to 225 days) (Figs. 2b, c). Since the corn had been pollinated, the male and female ears on the stigma, together with the silky hairs on the corn leaf sheaths, desiccated and turned yellow, resulting in a decreased LAI. While rice and soybeans remain green or yellow-green with sufficient water at this stage. In comparison to trees, the variations in stem, leaf, and morphology led to a decreased LAI (Fig. 2d). Nonetheless, these discrepancies progressively diminish as corn grows. Furthermore, tree greening occurs earlier than corn emergence, browns later than corn maturity, and exhibits denser canopy coverage with extended phenological period (Zhao et al., 2023). Compared with grassland and wetland (Figs. 2e, f), corn has a greater LAI than grass during the whole growing season. However, during EMV3 to V7 (130 to 160 days), the LAI of corn was inferior to that of wetlands. This is because the vegetation in the wetlands is perennial, and its greening rate is surpasses the growth rate of corn. The LAI differences are primarily associated with phenological shifts, (Figs. 2b, c, f).

### 3.2. Comparison of LST changes in various phenological stages and the whole growing season

Over the whole growing season, the conversion of rice, tree, grass, and wetland showed potential warming effects, whereas the conversion of soybean showed potential cooling effects in Mean_LST and Day_LST (Figs. 3a, b). Specifically, the largest increase in Day_LST occurred when corns were converted into trees (0.92±0.33 K), followed by rice (0.86 ±0.24 K), grasslands (0.06±0.35 K), and wetlands (0.06±0.23 K), respectively (Fig. 3a). The conversion of soybeans displayed cooling effect of −0.42±0.23 K in Day_LST. Night_LST cooling was observed in the conversions of rice (−0.49±0.14K ), wetlands (−0.22±0.15K ), trees (−0.15±0.18K ), and soybean (−0.14±0.22K ) (Fig. 3c), while slight warming occurred in the conversions of grassland (0.08±0.19 K). Therefore, the increase in DTR_LST when corns were converted into rice (1.23±0.16 K), trees (1.08±0.78 K), wetlands (0.34±0.18 K), and grasslands (0.08±0.19 K), yet it decreased by −0.28±0.37 K when converted from corn to soybeans (Fig. 3d). The largest increase in Mean_LST occurred when corns were converted into trees (0.26±0.15 K), followed by rice (0.18±0.10 K), grasslands (0.06±0.14 K), wetland (0.01±0.13 K), respectively (Fig. 3b). The study provides satellite-based evidence of the LST change resulting from corn expansion in northeast China.

Interestingly, except for soybean, the ΔMean_LST of corn expansion initially decreased and subsequently increased in response to phenological shifts (Fig. 4). Specifically, the potential warming effect was significant during EMV3-V7 and V7-JD, with the largest warming in Mean_LST occurred when corns were converted into trees (1.24±0.43K ) (0.93±0.29 K), followed by grass (0.47±0.37 K) (0.43±0.31 K), rice (0.46±0.23 K) (0.31±0.22 K), wetlands (0.16±0.21 K) (0.15±0.34), respectively (Figs. 4f, g, h, i, m). Moreover, a slight cooling effect was observed during TD to MID in rice (−0.21±0.16 K), soybeans (−0.02 ±0.15 K), tree (−0.10±0.20 K), grass (−0.36±0.29 K), and wetland (−0.22±0.17 K) conversion. This indicated that the warming effect from EMV3 to JD dominated the Mean_LST changes over the whole growth season. The conversion of soybeans demonstrated considerable potential cooling, with the cooling effect from EMV3 to JD surpassing warming effects from MID to MD (Fig. 4g, i). The △DTR_LST and Day_LST displayed comparable patterns with Mean_LST in various phenological stages. In conclusion, phenological shifts regulated the change in LST associated with corn expansion, regardless of the conversion types.

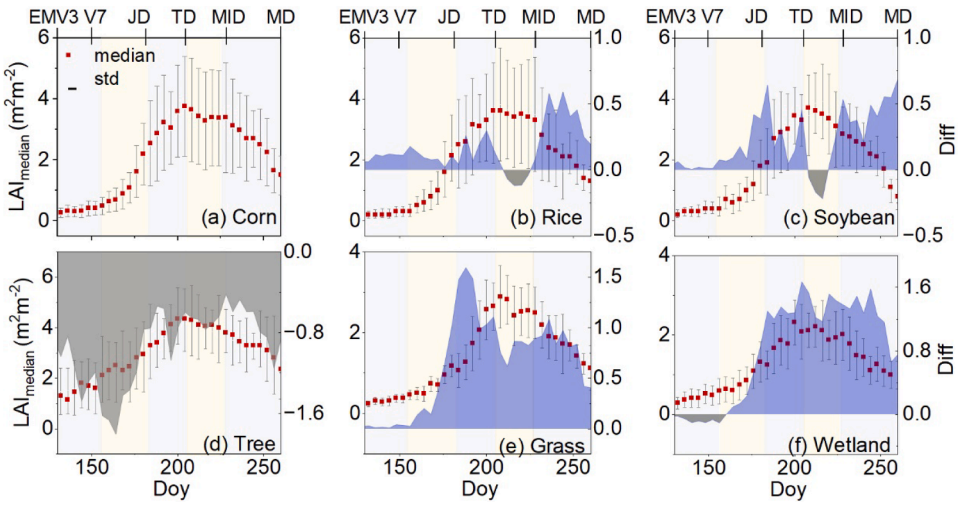


**Fig. 2.** Comparison of LAI among corn (a) and rice (b), soybean (c), tree (d), grass (e), and wetland (f) during the crop growing season. Gray indicates that corn has a lower LAI than other vegetation, and purple indicates that corn has a higher LAI than other vegetation. EMV3, V7, JD, TD, MID, and MD represent the three-leave date, seven-leave date, jointing date, tassel date, milky date, and maturity date, respectively.

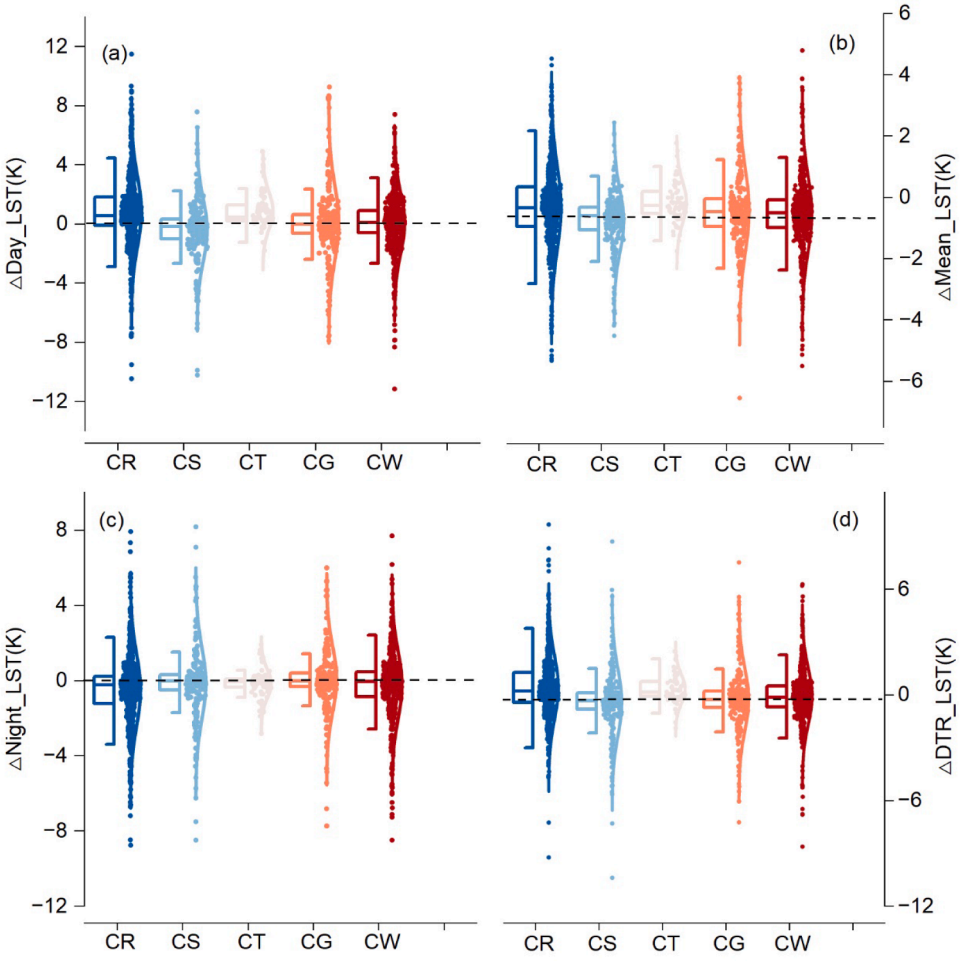


**Fig. 3.** Differences in average land surface temperatures (LSTs) between corn and rice, soybean, tree, grass, and wetland during the whole growing period of corn (WGP, from EMV3 to MD) from 2017 to 2019. The differences of (a) Day_LST, (c) Night_LST, and (b) Mean_LST as well as (d) diurnal temperature range (DTR) between pure corn pixels and the adjacent pure rice pixels (CR), pure soybean pixels (CS), pure tree pixels (CR), pure grass pixels (CG), and pure wetland pixels (CW) in northeast China. The middle lines represent the median values of ΔLSTs. The uncertainties are at a 95 % confidence level. The detailed values are displayed in Tables S3-S7.

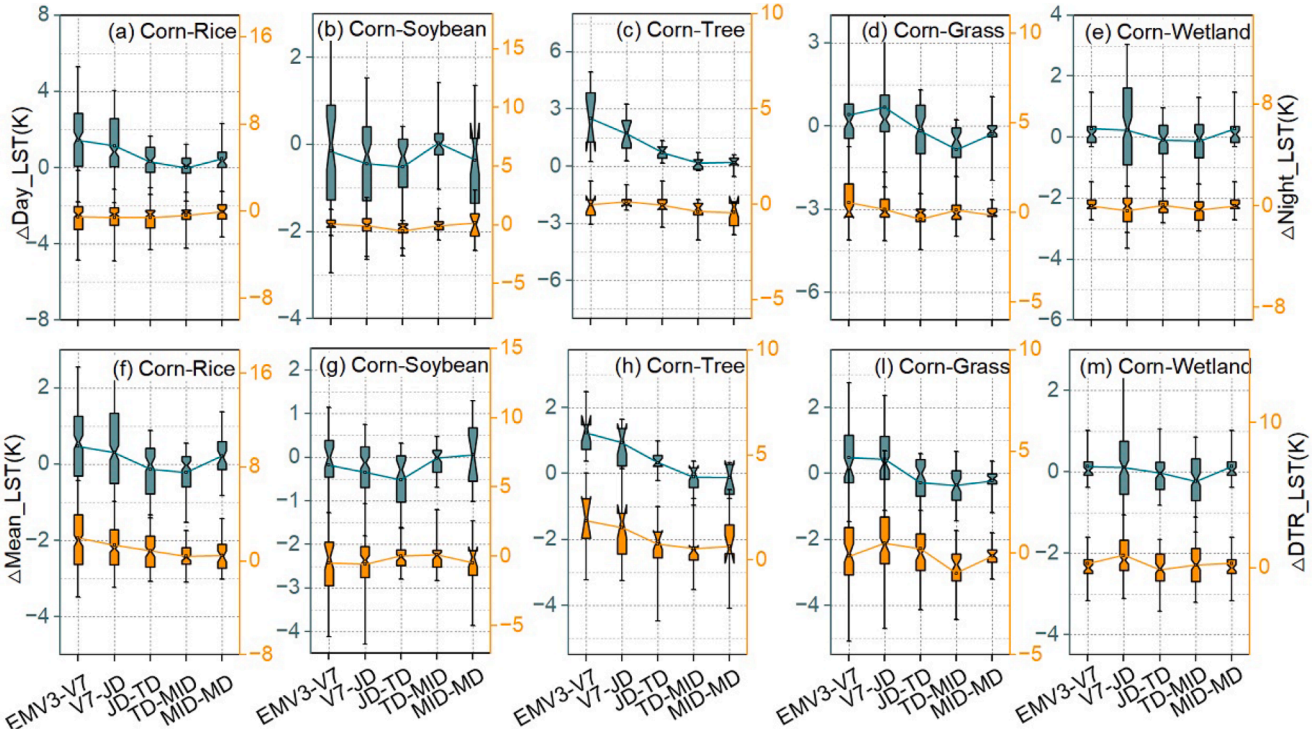


**Fig. 4.** Comparison of LST between corn and rice, soybean, tree, grass, and wetland in various phenological stages from 2017 to 2019. The differences of Day_LST, Night_LST, and daily Mean_LST as well as DTR_LST between pure corn pixels and the adjacent pure rice pixels (a), pure soybean pixels (b), pure tree pixels (c), pure grass pixels (d), and pure wetland pixels (d) in northeast China, respectively. The uncertainties are in a 95 % confidence level. The detailed values are displayed in Tables S3-S7.

The effect of phenological stages on LST varies according to latitude (from north to south). The ΔDTR_LST and ΔDay_LST displayed consistent trends in latitude and phenological stages across five vegetation conversion types. ΔDTR_LST and ΔDay_LST exhibited higher variations than ΔMean_LST and ΔNight_LST (Figs. 5, 6). The warming effect of Day_LST increased with latitude in rice, tree, and grassland conversion types during EMV3-V7 (Figs. 5 a1, c1, d1). Subsequently, the warming trend of ΔDay_LST gradually slowed down and even exhibited cooling with the phenology shift. For example, during TD-MID, ΔDay_LST decreased with increasing latitude in the conversion of trees and grasslands (Figs. 5 c4, d4). ΔDay_LST in wetland and soybean conversion types are more complex. During EMV3-V7 and V7-JD, the ΔDay_LST of soybean conversion displayed cooling at 46°N-47°N and warming at 48°N −49°N (Figs. 5 b1, b2), potentially linked to the differential growth of corn and soybean across different latitudes. During EMV3-V7, the ΔDay_LST of wetland conversion reveals a cooling trend

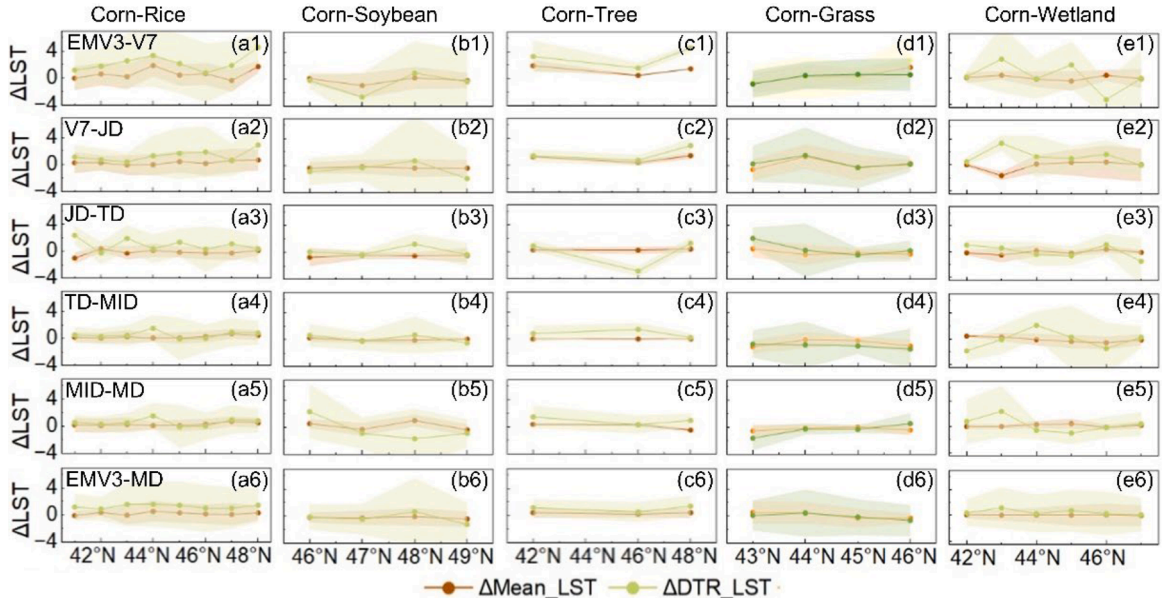


**Fig. 5.** Variation of ΔDay_LST, and ΔNight_LST with latitude in various phenological stages and the whole growing season. Lightly shaded areas in panels represent all samples' standard deviation (SD).

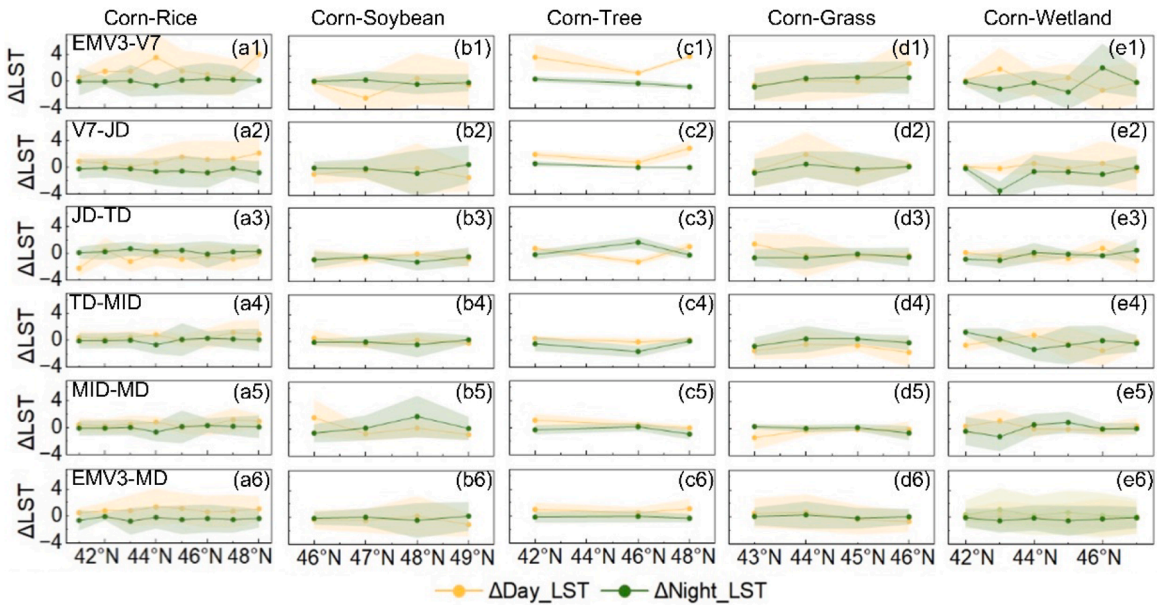


**Fig. 6.** Variation of ΔMean_LST, and ΔDTR_LST with latitude in various phenological stages and the whole growing season. Lightly shaded areas in panels represent all samples' standard deviation (SD).

at 44°N-46°N and a warming trend at 42°N-44°N (Fig. 5 e1). This could be owing to higher air temperatures at lower latitudes, which facilitate the growth of natural vegetation on wetlands, thus replacing wetlands with emerging corn, resulting in a warming effect.

### 3.3. Biophysical mechanism of LST variation in various phenological stages

To understand the driving mechanisms of LST variations from the corn expansion. First, this study compared the albedo and *f* changes in various phenological stages (Fig. 7). Second, this study utilized a temperature response model to estimate the △LST (Eq. (3)). The LST variations were attributed to the individual radiative (Albedo-induced △LST), non-radiative local forcing mechanisms (*f*-induced △LST), and the change in heat conducted by the surface medium ($\Delta T_s$_$G$) (Fig. 8). $\Delta T_s$_$G$ not explained in follow due to its insignificant magnitudes (Bright et al., 2017).

Fig. 8 illustrated that the △LST_Cal was consistent with the △LST_Obs in various phenological stages. The ΔLST_Cal's accuracy ranged from 0.74 to 0.94 across various vegetation cover conversions, with all results statistically significant at the 0.05 level (Fig. S1), indicating that the two components of the temperature responses including the albedo change (△LST_Alb) and energy redistribution factor change (△LST_f) better reflect the radiative and nonradiative process in regulating LST.

Various phenological stages regulated the changes in biophysical forcings of surface energy balance in five vegetation types converted to corn (Fig. 7). EMV3 to JD dominated the temperature effect on Mean_LST for the whole growth season. Because the warming effects in EMV3 to JD were stronger than the cooling effects in TD to MD for rice, grass, and trees. The cooling effects in EMV3 to JD were stronger than the warming effects in TD to MD for soybeans. Specifically, from EMV3 to JD, the marked increase in mean *f* was observed in vegetation types conversions, such as trees (0.92±0.50), followed by wetlands (0.49 ±0.39), rice (0.43±0.36), and grass (0.19±0.42) (Figs. 7a, c, e, g, i), with a slight decrease in soybeans (0.05±0.12). The decrease in mean albedo was observed in the conversion of rice, trees, and wetlands, while a slight increase was observed in grass and soybeans at this stage (Figs. 7b, d, f, h, j). A higher albedo indicates that the surface reflects more radiation and dissipates more energy, controlling the incoming energy in the surface energy balance (Lee et al., 2011). A higher *f* value indicates that vegetation ecosystems are more efficient in dissipating energy from the surface owing to their intrinsic biogeophysical properties (Bright et al., 2017; Lee et al., 2011). It is regarded as a relevant indicator of vegetation's structural and physiological controls on the surface energy balance, which can be divided into a combined effect of evaporation and turbulent heat exchange. Therefore, the △LST contributions of non-radiative forcing caused by *f* changes were 1.97±0.88 K (trees), 1.55±1.12 K (rice), 0.87±0.45 K (grass), 0.32±0.34 K (wetlands), and 0.12±0.32 K (soybeans). The △LST contributions of radiative forcing induced by albedo change were −0.03±0.10 K (trees), −0.35±0.20 K (rice), 0.15±0.19 K (grass), −0.03±0.10 K (wetlands), and −0.09±0.20 K (soybeans) (Fig. 8). Non-radiative warming effect surpassed radiative cooling effect, dominated the LST change at EMV3 to JD. While in TD to MID, the denser corn canopy exhibited increased evapotranspiration compared to rice, soybean, and grass, resulting in a cooling effect of non-radiative forcings (Figs. 8a, b, d). Furthermore, the albedo of trees produced a radiative cooling effect in JD to MD, contrasting with radiative warming effect observed from EMV3 to JD. The result suggested that the phenological shifts regulate the warming and cooling effects resulting from albedo-induced radiative forcing as well as *f* induced non-radiative processes.

The LST change governed by both non-radiative and radiative processes, is influenced by latitude and phenological stages (Fig. 9). The LST changes caused by radiative and non-radiative processes in rice and wetland conversions at 42°N-44°N exhibit consistent trends, particularly during EMV3-V7. They exhibited the most pronounced radiative cooling and non-radiative warming effect at 43°N (Figs. 9 a1, e1). During V7-JD and MID-MD, the non-radiative warming effect of wetland conversion surpassed that of rice conversion, correlating with increasing latitude (44°N-47°N). This indicated that the conversion of wetlands to corn results in stronger warming at higher latitudes. The warming effect of grassland decreased with rising latitude (Fig. 9 d6). The warming effect produced by tree conversion initially decreased and then increased with latitude. The non-radiative warming effect of EMV3-JD offsets the radiative cooling of JD-MID, which predominates the ultimate temperature change (Figs. 8, 9). Furthermore, the LST changes were no significant difference in latitude for soybean conversion throughout the EMV3-MD (Fig. 9 b6). However, in EMV3-V7 and MID-

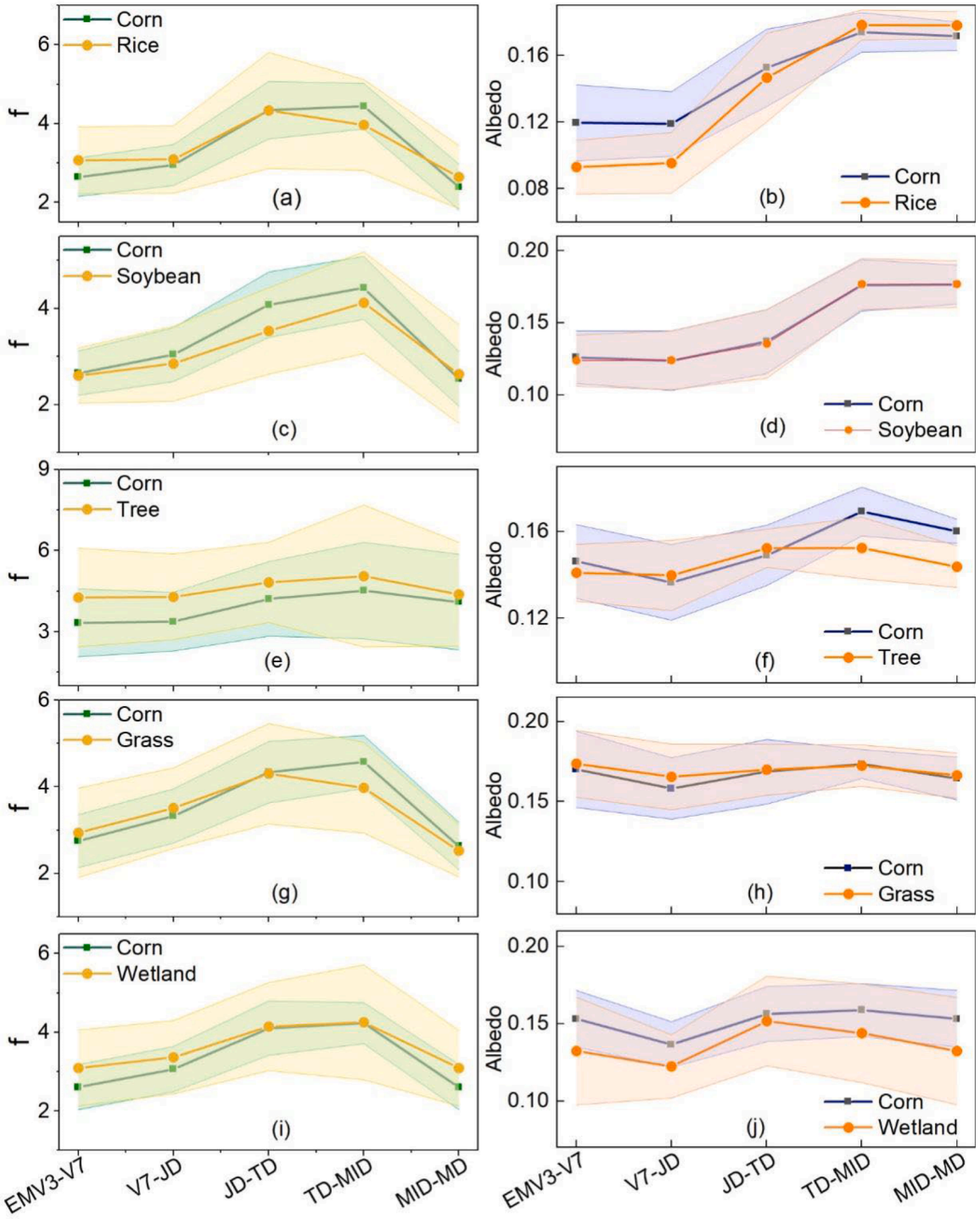


**Fig. 7.** Albedo and energy redistribution factor (*f*) in various phenological stages from 2017 to 2019. The daily value of albedo (a, c, e, g, and i) and *f* (b, d, f, h, and j) for corn, rice, soybean, tree, grass, and wetland within adjacent sample areas. Lightly shaded areas in panels represent all samples' standard deviation (SD).

MD, there is an obvious latitude fluctuation in LST changes, which could be correlated with air temperature changes, or the sowing and ripening-date of corn and soybean. For example, soybeans could be sown later in higher latitudes, so they grow more slowly during the EMV3-V7 stage of corn. On the other hand, higher latitudes have lower air temperatures, which affect crop growth and result in larger differences in biophysical properties, making the LST change more significant.

## 4. Discussion

### *4.1. The importance of phenology in regulating surface biophysical processes*

Detailed phenological information provides a new perspective for investigating the LST change in corn expansion. Phenology reflects the biophysical characteristics of crops from sowing to harvest (Ma et al., 2023). It more accurately describes the changes in surface physiological structure. Owing to the focus on equidistant time scale such as months,

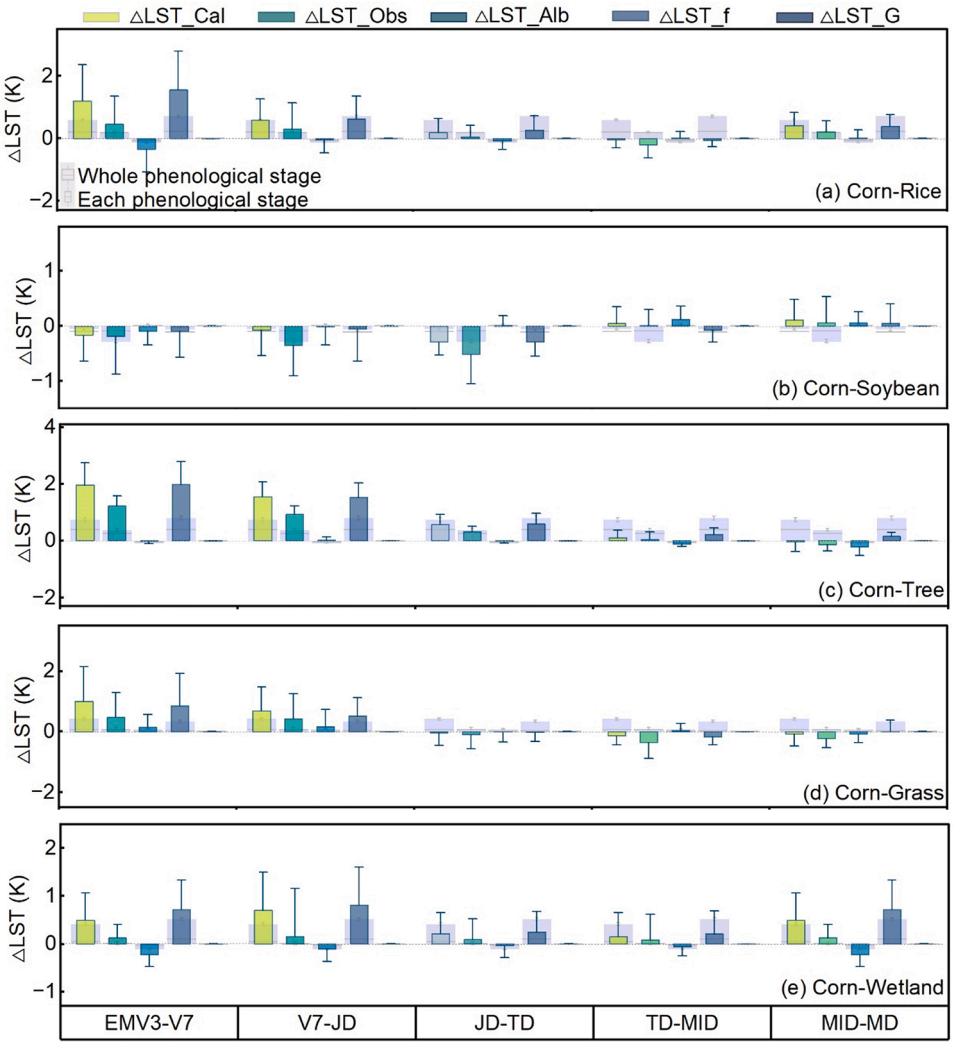


**Fig. 8.** Comparison of the biophysical effect at the whole growing period and various phenological stages between corn and land surfaces (within 5 km) from 2017 to 2019. a, Corn and Rice; b, Cron and Soybean; c, Corn and Tree; d, Corn and Grass, e, Corn and Wetland. Error bars are given as one SD for the clusters of all samples.

seasons, and years (Bright et al., 2017; Lee et al., 2011; Liao et al., 2018; Liu et al., 2018; Zhang et al., 2023b) of prior studies, there has been a limitation of analyses into biophysical effects on LST. For instance, Liu et al. (2022) and Liu et al. (2019b) revealed that the △LST between irrigated rice fields and rain-fed fields in different months constrained changes in physiological structure-induced surface biophysical processes. More detailed phenological stages facilitate the understanding of variations in biophysical process throughout crop growth. This study also compared △LST and its biophysical mechanisms across various phenological stages and whole growth seasons with latitude changes. The result indicated that non-radiative processes from EMV3 to JD dominated the warming effect of corn expansion (Fig. 8), and the impact of phenological stages on LST varies with latitude (from north to south) (Figs. 5,6). These were not assessed in previous studies (Liu et al., 2019a; 2022).

Furthermore, phenological shifts governed the radiative and non-radiative processes with varying magnitudes and directions (Fig. 8). Phenological shifts affected LAI change, which is crucial in regulating biophysical feedback mechanisms (Kala et al., 2014) by modulating the absorption of solar radiation through alterations in albedo and evapotranspiration. The latent heat fluxes increase with crop growth and reach their peak when the canopy achieves maximum LAI (Bohm et al., 2020). Upon maturity, brown crops exhibit a greater albedo and absorb less solar radiation than bare soil and green vegetation, resulting in lower LST (Sacks and Kucharik, 2011). Consequently, analyzing water and energy allocation across various phenological stages is essential for revealing the biophysical mechanisms underlying corn expansion.

### 4.2. *The driving mechanism of regional LST change*

This study found a potential cooling effect during the EMV3 to TD for soybean conversion attributed to the decrease in Day_LST and Night_LST. This is probably due to the higher height of corn stalks compared to soybeans stalks, as well as the wider and thicker leaves of corn. The corn roots need to absorb more soil moisture to supply transpiration, hence decreasing Day_LST. Then the reduced Day_LST and shading from the stems and leaves diminish soil heat storage, resulting in a decrease in the Night_LST (Lee et al., 2011; Pelech et al., 2021; Yu et al., 2022). This indicated that the biophysical effects of corn expansion were reversed in phenological shifts as its structural and functional development progressed. For example, soybean conversion led to substantial cooling effects from the EMV3 to TD (−0.19±0.46 K) (−0.35 ±0.21 K) (−0.52±0.35K ), followed by slight warming from TD to MID (0.04±0.46 K), and cooling from MID to MD (−0.08±0.13 K). Likewise, the grasslands conversion led to notable warming effects from the EMV3 to JD (0.47±0.37K ) (0.43±0.31 K), followed by cooling from JD to MD (−0.27±0.32 K) (−0.36±0.29 K) (−0.23±0.19 K). Grasslands are perennial natural vegetation that greening earlier than crops by

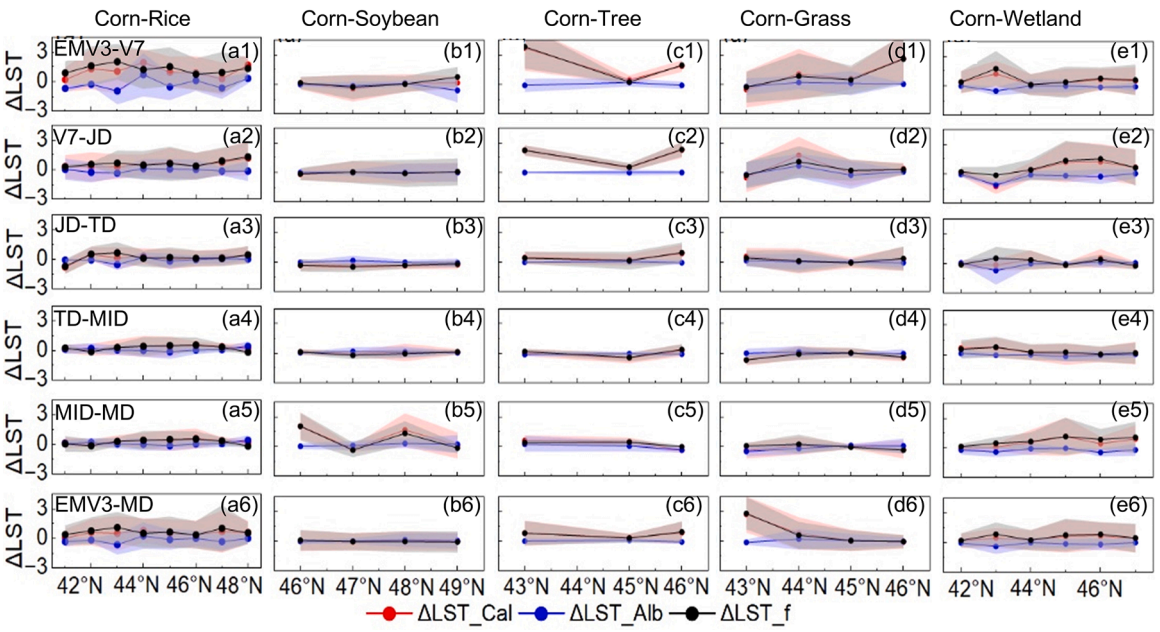


**Fig. 9.** Variation of ΔLST_Cal, ΔLST_Alb, and ΔLST_f with latitude in various phenological stages and the growing season. Lightly shaded areas in panels represent all samples' standard deviation (SD).

approximately 20 days (Zhao et al., 2023). During EMV3 to JD, the corn plants are diminutive, mainly displayed bare black soil background, which exhibits lower albedo and evaporation compared to natural vegetation (Yu et al., 2022). Consequently, both radiative and non-radiative processes exhibited warming effects. During JD to MD, the grassland conversions caused biophysical cooling owing to the non-radiative and radiative cooling (Fig. 8d; Figs. 9 d4, d5).

Furthermore, this study revealed that corn expansion had significant biophysical warming potentials over the whole growth season when converting rice, trees, grass, and wetlands (Fig. 8), in agreement with previous remote sensing studies on LST changes (Duveiller et al., 2018; Zhou et al., 2021). However, the potential warming effect gradually decreases with phenological shifts. For example, although the trees converted to corn consistently produced a warming effect, the amplitude steadily decreased in various phenological stages. (Fig. 8c). These could be related to the intrinsic biogeophysical properties, as phenological shifts influence vegetation structural and physiological, hence controlling the surface energy balance. The non-radiative warming effect decreased during JD to MD is likely attributable to increased surface roughness associated with corn grows, leading to enhanced energy diffusion via turbulence (Chen et al., 2020; Lee et al., 2011). In other words, as the LAI disparity between corn and trees decreases (Fig. 2), the difference in evapotranspiration also decreases, leading to a weaker non-radiative effect. In contrast, non-radiative cooling between corn and grass intensifies (Fig. 8d), presumably due to the greater height and coarser surface of corn, facilitating heat transfer from the surface to the atmosphere via turbulence. It illustrated that the radiative and non-radiative mechanisms of vegetation undergo continuous change during the growth season. Overall, coupled vegetation-climate modeling needs to account for specific phenological stages and vegetation cover types.

The LST change regulated by both non-radiative and radiative processes, is influenced by latitude (Fig. 9). The LST changes caused by radiative and non-radiative processes in rice and wetland conversions at 42°N-44°N exhibit consistent trends, particularly during EMV3-V7 (Figs. 9 a1, e1), where non-radiative processes predominantly surpassed radiative processes, thereby influencing the biophysical warming effect (Figs. 8a, e; Figs. 9 a1, e1). During V7-JD and MID-MD, the non-radiative warming effect of wetland conversion surpassed that of rice conversion as latitude increased from 44°N to 47°N. This indicates that the conversion of wetlands causes more pronounced warming effects compared to conversion of rice in high latitudes. This was a novel finding compared to previous studies that mainly focused on rice as an artificial wetland able to alleviating the warming impacts of wetland degradation (Liu et al., 2019a, 2022). Moreover, non-radiative warming exists in two conversion types, and radiative cooling also exists in the wetland conversion with the latitude change (Figs. 9 b2, e2) from the V7 to JD. However, radiative forcing warms the LST of the rice conversion at 44°N-46°N (Fig. 9 b2). The sign of the radiation processes controlling LST was contrary. That could be attributed to the wetlands exhibiting a lower albedo than that of corn and rice in these regions. During MID to MD, the non-radiative and radiative warning LST for rice conversion, whereas no-radiative warming outweighed radiative cooling still dominant the LST from wetland conversion at this stage. Therefore, biophysical mechanisms controlling rice and wetlands LST were not synchronized.

### 4.3. *Uncertainties and limitations*

The accuracy of the vegetation-type map and the spatial resolution of the ERA5_land could lead to uncertainties. This research utilized the intersection of two datasets to determine the ultimate vegetation type, minimizing misclassification of high spatial resolution (10–30 m) vegetation type maps. For example, the spatial location of grass and trees is the intersection of ESRI_LULC and CLCD. Moreover, this study investigated the biophysical mechanisms underlying the effects of corn expansion at different phenological stages on LST, rather than across a temporal scale of months or years. To accurately describe energy within phenology, ERA5_land data with one-day resolution is required. Nonetheless, this could underestimate the effect of corn expansion on LST due to sacrificing the spatial resolution (0.1°). Because of the spatial heterogeneity decrease of $L_{\downarrow}$, $S$, and $T_a$, resulting in an underestimate of $R_n^*$.

This study contributes to the current understanding of the impact for phenological shifts on LST changes in corn expansion. Our analysis using the temperature response model to decompose the LST change resulting from corn expansion attributed to albedo and the $f$ (Bright et al., 2017; Liu et al., 2022). Aerodynamic resistance primarily correlates with surface roughness and iscrucial in governing the energy transfer

between the land surface and the atmosphere (Chen et al., 2020; Yu et al., 2022; Zhang et al., 2022). Therefore, the contribution of more biophysical factors on changes in LST could be quantified using the semi-mechanistic empirical model and regional or global climate models (Zeng et al., 2017; Zhang et al., 2023a), particularly as the station observation network expands and as new remote sensing products are available in the future. Furthermore, given the importance of phenology in regulating LST during corn expansion, future studies should investigate the direct temporal trends and relative contributions of corn expansion and phenology changes to LST.

## 5. Conclusion

This study utilized the pair-wise comparison approach and the temperature response model to investigate the biophysical effect of corn expansion on local LST in various phenological stages and latitudes, using remote sensing observational data over northeast China,. The results indicated that the conversion of trees, grass, rice, and wetlands produced the warming effect in the Mean_LST, whereas the conversion of soybeans cooled the Mean_LST. Because EMV3 to JD dominated non-radiative warming in ΔMean_LST at rice, tree, grass, and wetlands conversions, and non-radiative cooling in ΔMean_LST for soybean conversion. Therefore, LST changes of corn expansion were influenced by various phenological stages, which dominated non-radiative processes with varying signs and magnitudes. Moreover, the effect of phenological stages on LST varies with latitude. During V7-JD and MID-MD, the non-radiative warming effect of wetland conversion surpassed that of rice conversion as latitude increased (44°N-47°N). This indicated that the conversion of wetlands caused intensified warming at high latitudes in these stages. Our findings highlight the importance of accounting for phenology shifts regulating biophysical mechanisms with latitude changes for better quantification and understanding of the expansion's impact on climate, as well as for making effective adaptation and mitigation climate strategies in the future agroecosystem.

## CRediT authorship contribution statement

**Yuyang Ma:** Writing – review & editing, Writing – original draft, Visualization, Methodology, Investigation, Formal analysis, Conceptualization. **Jie Li:** Writing – review & editing. **Jianxi Huang:** Writing – review & editing, Conceptualization. **Anne Gobin:** Writing – review & editing. **Xuecao Li:** Writing – review & editing. **Wenqi Liu:** Methodology. **Haixiang Guan:** Formal analysis. **Nadezhda N. Voropay:** Writing – review & editing. **Chuli Hu:** Writing – review & editing.

## Declaration of competing interest

The authors declare that they have no known competing financial interests or personal relationships that could have appeared to influence the work reported in this paper.

## Acknowledgments

Acknowledgement for the data support from "National Earth System Science Data Center. (https://www.geodata.cn)".

## Supplementary materials

Supplementary material associated with this article can be found, in the online version, at doi:10.1016/j.agrformet.2024.110373.

## Data availability

Data will be made available on request.

## References

Abera, T.A., Heiskanen, J., Pellikka, P.K.E., Adhikari, H., Maeda, E.E., 2020. Climatic impacts of bushland to cropland conversion in Eastern Africa. Sci. Total. Environ. 717, 137255.
Bohm, K., Ingwersen, J., Milovac, J., Streck, T., 2020. Distinguishing between early- and late-covering crops in the land surface model Noah-MP: impact on simulated surface energy fluxes and temperature. Biogeosciences. 17, 2791–2805.
Bouvet, A., Mermoz, S., Le Toan, T., Villard, L., Mathieu, R., Naidoo, L., Asner, G.P., 2018. An above-ground biomass map of African savannahs and woodlands at 25m resolution derived from ALOS PALSAR. Remote Sens. Environ. 206, 156–173.
Bright, R.M., Davin, E., O'Halloran, T., Pongratz, J., Zhao, K., Cescatti, A., 2017. Local temperature response to land cover and management change driven by non-radiative processes. Nat. Clim. Chang. 7, 296–302.
Chai, L., Liu, A., Li, X., Guo, Z., He, W., Huang, J., Bai, T., Liu, J., 2024. Telecoupled impacts of the Russia–Ukraine war on global cropland expansion and biodiversity. Nat. Sustain. 7, 432–441.
Chen, C., Li, D., Li, Y., Piao, S., Wang, X., Huang, M., Gentine, P., Nemani, R.R., Myneni, R.B., 2020. Biophysical impacts of Earth greening largely controlled by aerodynamic resistance. Sci. Adv. 6 eabb1981.
Yang, K., He, J., Wenjun, T., Lu, H., Qin, J., Chen, Y., Li, X., 2015. China Meteorological Forcing Dataset (1979-2018). C. National Tibetan Plateau Data (Ed.): National Tibetan Plateau Data Center.
Duveiller, G., Hooker, J., Cescatti, A., 2018. The mark of vegetation change on Earth's surface energy balance. Nat. Commun. 9, 679.
Fang, S., Mao, K., Xia, X., Wang, P., Shi, J., Bateni, S.M., Xu, T., Cao, M., Heggy, E., 2021. A dataset of daily near-surface air temperature in China from 1979 to 2018. Earth. Syst. Sci. Data 1–37. *2021*.
Gong, Y., Yin, J., Wang, S., Yang, S., Li, D., Pan, X., 2022. Climatology of Northeast China cold vortices during the warm season: a comparison of ERA5 and MERRA-2 reanalyses. Int. J. Climatol. 42, 7071–7086.
Graven, H., Keeling, R., Piper, S., Patra, P., Stephens, B., Wofsy, S., Welp, L., Sweeney, C., Tans, P., Kelley, J., 2013. Enhanced seasonal exchange of CO2 by northern ecosystems since 1960. Science (1979) 341, 1085–1089.
Guan, H., Huang, J., Li, L., Li, X., Ma, Y., Niu, Q., Huang, H., 2022. A novel approach to estimate maize lodging area with PolSAR data. Ieee T. Geosci. Remote 60, 1–17.
He, J., Yang, K., Tang, W., Lu, H., Qin, J., Chen, Y., Li, X., 2020. The First High-Resolution Meteorological Forcing Dataset For Land Process Studies Over China, 7. Sci Data, p. 25.
Huang, N., Wang, Z., Liu, D., Niu, Z., 2010. Selecting sites for converting farmlands to wetlands in the Sanjiang Plain, Northeast China, based on remote sensing and GIS. Environ. Manage 46, 790–800.
Kala, J., Decker, M., Exbrayat, J.-F., Pitman, A.J., Carouge, C., Evans, J.P., Abramowitz, G., Mocko, D., 2014. Influence of leaf area index prescriptions on simulations of heat, moisture, and carbon fluxes. J. Hydrometeorol. 15, 489–503.
Karra, K., Kontgis, C., Statman-Weil, Z., Mazzariello, J.C., Mathis, M., Brumby, S.P., 2021. Global land use/land cover with Sentinel 2 and deep learning. In: 2021 IEEE international geoscience and remote sensing symposium IGARSS. IEEE, pp. 4704–4707.
Lee, X., Goulden, M.L., Hollinger, D.Y., Barr, A., Black, T.A., Bohrer, G., Bracho, R., Drake, B., Goldstein, A., Gu, L., Katul, G., Kolb, T., Law, B.E., Margolis, H., Meyers, T., Monson, R., Munger, W., Oren, R., Paw, U.K., Richardson, A.D., Schmid, H.P., Staebler, R., Wofsy, S., Zhao, L., 2011. Observed increase in local cooling effect of deforestation at higher latitudes. Nature 479, 384–387.
Levis, S., 2010. Modeling vegetation and land use in models of the Earth System. Wiley Interdiscipl. Rev. 1, 840–856.
Li, X., Zhou, Y., Asrar, G.R., Zhu, Z., 2018. Creating a seamless 1 km resolution daily land surface temperature dataset for urban and surrounding areas in the conterminous United States. Remote Sens. Environ. 206, 84–97.
Li, Z., Tan, J., Tang, P., Chen, H., Zhang, L., Liu, H., Wu, W., Tang, H., Yang, P., Liu, Z., 2016. Spatial distribution of maize in response to climate change in northeast China during 1980–2010. J. Geograph. Sci. 26, 3–14.
Liao, W., Rigden, A.J., Li, D., 2018. Attribution of local temperature response to deforestation. J. Geophys. Res. 123, 1572–1587.
Liu, F., Chen, Y., Shi, W., Zhang, S., Tao, F., Ge, Q., 2017. Influences of agricultural phenology dynamic on land surface biophysical process and climate feedback. J. Geograph. Sci. 27, 1085–1099.
Liu, T., Yu, L., Bu, K., Yan, F., Zhang, S., 2018. Seasonal local temperature responses to paddy field expansion from rain-fed farmland in the cold and humid sanjiang plain of China. Remote Sens. 10.
Liu, T., Yu, L., Zhang, S., 2019a. Impacts of wetland reclamation and paddy field expansion on observed local temperature trends in the sanjiang plain of China. J. Geophys. Res. 124, 414–426.
Liu, T., Yu, L., Zhang, S., 2019b. Land surface temperature response to irrigated paddy field expansion: a case study of Semi-arid Western Jilin Province, China. Sci. Rep. 9, 5278.
Liu, W., Dong, J., Du, G., Zhang, G., Hao, Z., You, N., Zhao, G., Flynn, K.C., Yang, T., Zhou, Y., 2022. Biophysical effects of paddy rice expansion on land surface temperature in Northeastern Asia. Agr. Forest Meteorol. 315.
Ma, Y., Shen, Y., Guan, H., Wang, J., Hu, C., 2023. A novel approach to detect the spring corn phenology using layered strategy. Int. J. Appl. Earth Obs. 122.
Man, W., Wang, Z., Liu, M., Lu, C., Jia, M., Mao, D., Ren, C., 2016. Spatio-temporal dynamics analysis of cropland in Northeast China during 1990-2013 based on remote sensing. Transac. Chin. Soc. Agr. Engineer. 32, 1–10.
Mao, D.H., Wang, Z.M., Du, B.J., Li, L., Tian, Y.L., Jia, M.M., Zeng, Y., Song, K.S., Jiang, M., Wang, Y.Q., 2020. National wetland mapping in China: a new product

resulting from object-based and hierarchical classification of Landsat 8 OLI images. Isprs J. Photogramm 164, 11–25.
McNicholl, B., Lee, Y.H., Campbell, A.G., Dev, S., 2021. Evaluating the reliability of air temperature from ERA5 reanalysis data. IEEE Geosci. Remote Sens. Lett. 19, 1–5.
Muñoz-Sabater, J., Dutra, E., Agustí-Panareda, A., Albergel, C., Arduini, G., Balsamo, G., Boussetta, S., Choulga, M., Harrigan, S., Hersbach, H., Martens, B., Miralles, D.G., Piles, M., Rodríguez-Fernández, N.J., Zsoter, E., Buontempo, C., Thépaut, J.-N., 2021. ERA5-Land: a state-of-the-art global reanalysis dataset for land applications. Earth. Syst. Sci. Data 13, 4349–4383.
Ning, J., Liu, J., Kuang, W., Xu, X., Zhang, S., Yan, C., Li, R., Wu, S., Hu, Y., Du, G., Chi, W., Pan, T., Ning, J., 2018. Spatiotemporal patterns and characteristics of land-use change in China during 2010–2015. J. Geograph. Sci. 28, 547–562.
Pelech, E.A., Alexander, B.C., Bernacchi, C.J., 2021. Photosynthesis, yield, energy balance, and water-use of intercropped maize and soybean. Plant Direct. 5, e365.
Piao, S., Liu, Q., Chen, A., Janssens, I.A., Fu, Y., Dai, J., Liu, L., Lian, X., Shen, M., Zhu, X., 2019. Plant phenology and global climate change: current progresses and challenges. Global Change Biol. 25, 1922–1940.
Román, M.O., Schaaf, C.B., Lewis, P., Gao, F., Anderson, G.P., Privette, J.L., Strahler, A. H., Woodcock, C.E., Barnsley, M., 2010. Assessing the coupling between surface albedo derived from MODIS and the fraction of diffuse skylight over spatially-characterized landscapes. Remote Sens. Environ. 114, 738–760.
Sacks, W.J., Kucharik, C.J., 2011. Crop management and phenology trends in the U.S. Corn Belt: impacts on yields, evapotranspiration and energy balance. Agr. Forest Meteorol. 151, 882–894.
Schaaf, C.B., Gao, F., Strahler, A.H., Lucht, W., Li, X., Tsang, T., Strugnell, N.C., Zhang, X., Jin, Y., Muller, J.-P., Lewis, P., Barnsley, M., Hobson, P., Disney, M., Roberts, G., Dunderdale, M., Doll, C., d'Entremont, R.P., Hu, B., Liang, S., Privette, J. L., Roy, D., 2002. First operational BRDF, albedo nadir reflectance products from MODIS. Remote Sens. Environ. 83, 135–148.
Shuai, Y., Schaaf, C.B., Strahler, A.H., Liu, J., Jiao, Z., 2008. Quality assessment of BRDF/albedo retrievals in MODIS operational system. Geophys. Res. Lett. 35.
Wan, Z., 2014. New refinements and validation of the collection-6 MODIS land-surface temperature/emissivity product. Remote Sens. Environ. 140, 36–45.
Wang, J., Xiao, X., Basara, J., Wu, X., Bajgain, R., Qin, Y., Doughty, R.B., Iii, B.M., 2021. Impacts of juniper woody plant encroachment into grasslands on local climate. Agr. Forest Meteorol. 307, 108508.
Wang, M., Mao, D., Wang, Y., Xiao, X., Xiang, H., Feng, K., Luo, L., Jia, M., Song, K., Wang, Z., 2023a. Wetland mapping in East Asia by two-stage object-based Random Forest and hierarchical decision tree algorithms on Sentinel-1/2 images. Remote Sens. Environ. 297.
Wang, M., Mao, D., Xiao, X., Song, K., Jia, M., Ren, C., Wang, Z., 2023b. Interannual changes of coastal aquaculture ponds in China at 10-m spatial resolution during 2016–2021. Remote Sens. Environ. 284.
Xin, Y., Lu, N., Jiang, H., Liu, Y., Yao, L., 2021. Performance of ERA5 reanalysis precipitation products in the Guangdong-Hong Kong-Macao greater bay area, China. J. Hydrol. 602, 126791.
Yang, J., Huang, X., 2021. The 30 m annual land cover dataset and its dynamics in China from 1990 to 2019. Earth. Syst. Sci. Data 13, 3907–3925.
Yang, K., He, J., Tang, W., Qin, J., Cheng, C.C., 2010. On downward shortwave and longwave radiations over high altitude regions: observation and modeling in the Tibetan Plateau. Agr. Forest Meteorol. 150, 38–46.
Yang, W., Tan, B., Huang, D., Rautiainen, M., Shabanov, N.V., Wang, Y., Privette, J.L., Huemmrich, K.F., Fensholt, R., Sandholt, I., 2006. MODIS Leaf Area Index products: From validation to Algorithm Improvement. Ieee T. Geosci. Remote 44, 1885–1898.
You, N.S., Dong, J.W., Huang, J.X., Du, G.M., Zhang, G.L., He, Y.L., Yang, T., Di, Y.Y., Xiao, X.M., 2021. The 10-m crop type maps in Northeast China during 2017-2019. Sci. Data 8.
Yu, L., Liu, Y., Yang, J., Liu, T., Bu, K., Li, G., Jiao, Y., Zhang, S., 2022. Asymmetric daytime and nighttime surface temperature feedback induced by crop greening across Northeast China. Agr. Forest Meteorol. 325.
Zeng, Y., Hao, D., Park, T., Zhu, P., Huete, A., Myneni, R., Knyazikhin, Y., Qi, J., Nemani, R.R., Li, F., Huang, J., Gao, Y., Li, B., Ji, F., Köhler, P., Frankenberg, C., Berry, J.A., Chen, M., 2023. Structural complexity biases vegetation greenness measures. Nat. Ecol. Evol. 7, 1790–1798.
Zeng, Z., Piao, S., Li, L.Z.X., Zhou, L., Ciais, P., Wang, T., Li, Y., Lian, X., Wood, E.F., Friedlingstein, P., Mao, J., Estes, L.D., Myneni, Ranga B., Peng, S., Shi, X., Seneviratne, S.I., Wang, Y, 2017. Climate mitigation from vegetation biophysical feedbacks during the past three decades. Nat. Clim. Chang. 7, 432–436.
Zhang, C., Dong, J., Leng, G., Doughty, R., Zhang, K., Han, S., Zhang, G., Zhang, X., Ge, Q., 2023a. Attenuated Cooling Effects With Increasing Water-Saving irrigation: Satellite evidence from Xinjiang, China. Agr. Forest Meteorol. 333.
Zhang, C., Ge, Q., Dong, J., Zhang, X., Li, Y., Han, S., 2023b. Characterizing spatial, diurnal, and seasonal patterns of agricultural irrigation expansion-induced cooling in Northwest China from 2000 to 2020. Agr. Forest Meteorol. 330.
Zhang, Z., Lin, A., Zhao, L., Zhao, B., 2022. Attribution of local land surface temperature variations response to irrigation over the North China Plain. Sci. Total. Environ. 826, 154104.
Zhao, G., Dong, J., Yang, J., Wang, H., Dai, J., Zhou, Y., Cui, Y., Ge, Q., 2023. Cropland expansion delays vegetation spring phenology according to satellite and in-situ observations. Agric. Ecosyst. Environ. 356.
Zhou, D., Xiao, J., Frolking, S., Liu, S., Zhang, L., Cui, Y., Zhou, G., 2021. Croplands intensify regional and global warming according to satellite observations. Remote Sens. Environ. 264.